AGU PUBLICATIONS

Space Weather

RESEARCH ARTICLE
10.1002/2014SW001129

Key Points:
- Thumba and Sriharikota ionosondes from Indian sector have been utilized
- Investigation on the F layer height rise and ESF onset time has been presented
- Observations highlight the important role of LSWS in ESF

Correspondence to:
L. M. Joshi,
lmjoshinarl@gmail.com

Citation:
Joshi, L. M., S. Balwada, T. K. Pant, and S. G. Sumod (2015), Investigation on *F* layer height rise and equatorial spread *F* onset time: Signature of standing large-scale wave, *Space Weather*, *13*, doi:10.1002/2014SW001129.

Received 2 OCT 2014
Accepted 2 MAR 2015
Accepted article online 6 MAR 2015

Investigation on *F* layer height rise and equatorial spread *F* onset time: Signature of standing large-scale wave

Lalit Mohan Joshi[1], S. Balwada[2], T. K. Pant[3], and S. G. Sumod[4,5]

[1]Indian Institute of Geomagnetism Mumbai, Mumbai, India, [2]National Atmospheric Research Laboratory, Chittoor, India, [3]Vikram Sarabhai Space Centre, ISRO, Thiruvananthapuram, India, [4]Laboratório de Fisica e Astronomia, UNIVAP, São Paulo, Brazil, [5]Department of Physics, Sacred Heart College, Kochi, India

Abstract Equatorial spread *F* observations have been categorized into three categories based on ionograms recorded over Sriharikota. First category comprised cases where the onset of equatorial spread *F* (ESF) was concurrent with the peak *h'F* time. Second and third categories comprised cases where the onset of ESF happened with a delay of 30 min and more than 30 min, respectively, with reference to the peak *h'F* time. Average peak *h'F* in the first category was more than 35 km higher than that in the second and third categories. Also, the peak vertical (upward) plasma drift was higher in the first category. Assuming the genesis of *F* region irregularity to have happened at or before the time of *F* layer attaining the peak height, late onset of ESF indicates the genesis of irregularities to have happened westward of Sriharikota. The fact that the peak *h'F* values were remarkably different in the three categories indicates a zonal variation of eastward electric field and postsunset height rise of *F* layer. The relative magnitude of the *F* layer height rise in the three different categories over Sriharikota has also been found to be significantly different than that over Thumba, an equatorial (magnetic) station located ~360 km westward of Sriharikota longitude. This scenario points toward the existence of a large-scale zonal standing wave in the *F* layer and its important role in *F* region instability process. Results presented in the manuscript have been discussed in the light of current understanding on the large-scale wave structure.

1. Introduction

Day-to-day variability of the equatorial spread F (ESF) continues to be a puzzle even decades after the first scientific investigation was carried out to reveal its existence and behavior. It refers to the unusually large spread in the *F* region echo trace seen on the ionosonde, a swept frequency pulsed radar. It constitutes an important aspect of ionospheric weather and affects satellite based navigation and communication applications. Although we know that the main cause of this enigmatic phenomenon is the generation of the equatorial plasma bubble (EPB), several interesting aspects of it have not been fully understood. One such aspect is the large-scale spatial modulation in its occurrence. Large-scale wave structure (LSWS), originating in the *F* region during the evening hours has been considered to be the main cause of it [*Tsunoda and White*, 1981]. It is being believed that the day-to-day variability of the ESF is controlled by the occurrence and the behavior of the LSWS.

LSWS and its role in the formation of plasma bubble have been studied using a variety of observational tools, which include incoherent scatter radar [*Tsunoda and White*, 1981], ionosonde [*Tsunoda*, 2008, 2009], airglow photometer [*Patra et al*., 2013], and satellite measurement [e.g., *Thampi et al*., 2009; *Huang et al*., 2013]. Investigations carried out so far to study the role of LSWS in the formation of plasma bubble have mostly been in the form of case studies based on limited number of events [e.g., *Tsunoda and White*, 1981; *Tsunoda*, 2008, 2009; *Patra et al*., 2013; *Thampi et al*., 2009; *Huang et al*., 2013; *Tsunoda and Ecklund*, 2007], except the investigation by *Tulasi Ram et al*. [2014a], comprising ~70 days of observations from the African sector and 99 days of observations from the Asian sector. In fact, the actual role and importance of the LSWS in the onset of the ESF can only be ascertained by examining a long-term and continuous data set.

ESF not only remains to be a matter of scientific quest but also poses as a technological challenge in the field of satellite-based navigation and communication [*Shume et al*., 2013; *Bagiya et al*., 2013; *Oladipo et al*., 2014]. Several investigations in the recent times have highlighted the day-to-day variability in the ionospheric

irregularities [e.g., *Whalen*, 2007] and its impact on the satellite-based navigation through L band scintillation [e.g., *de Lima et al*., 2014; *Zhang et al*., 2010; *Sreeja et al*., 2011, 2012; *Aquino and Sreeja*, 2013]. Recently, *Kelly et al*. [2014] have highlighted how ESF can critically hamper real-time UHF communication. Thus, investigations on the causative mechanisms of the ESF are required, also from the technological perspectives. One of the potential causes of the ESF is the LSWS.

One of the most interesting features of the LSWS is the lack of zonal propagation with time [*Tsunoda and Ecklund*, 2007]. LSWS originates as a standing wave of plasma density in the *F* region, gains amplitude with time, and believed to result in the formation of plasma bubbles. This paper deals with the relation of the onset time of the equatorial spread *F* and the peak height attained by the *F* layer in the evening hours. If the postsunset height rise of the *F* layer is purely time dependent, the onset time of spread *F* and the peak height attained by the *F* layer will have no relationship. However, if the postsunset height rise of the *F* layer depends on time as well as the zonal location, spread *F* onset time can be related to the peak height attained by the *F* layer. Later scenario points toward the existence of the LSWS. This aspect has been discussed in details in this paper.

2. Data and Methodology

Ionosonde observations made during 15 February 2004 to 2 April 2004 period (48 days) from Sriharikota (13.7°N, 80.1°E, and 6.7°N magnetic latitude) and Thumba (8.53°N, 76.87°E, and 0.2°N magnetic latitude) in India have been used for the study presented in this paper. KEL IPS-42 digital ionosonde has been used for making the observations. Observations were made once every 15 min. Range resolution of the ionosonde was ~3 km. Observations were recorded digitally and were analyzed using the software supplied by the instrument manufacturer (KEL Aerospace), to derive the standard parameter like *h'F*. Vertical plasma drift of the *F* layer has been inferred by calculating the rate of change of *F* layer height ($V_Z = dh'F/dt$). During the entire observational period, the average $F_{10.7}$ was 110 solar flux unit. Of all the spread *F* nights discussed in this manuscript, two nights belonged to geomagnetically active period (2 and 11 March). A geomagnetic storm has also occurred on 9 March 2004 (refer to *Tulasi Ram et al*. [2008] and *Tulasi Ram et al*. [2014b]). Thus, the observation recorded on the night of 9 March 2004 has been excluded from the analysis presented in this manuscript, so as to focus primarily on the quite time variability of ESF. For detailed study we have divided the spread *F* cases based on ionograms recorded over Sriharikota into three categories: Category 1 (24 February and 6, 8, 19, 23–25, and 27 March), Category 2 (22 and 23 February and 11, 16, and 26 March), and Category 3 (21 February and 5, 13, 14, 20, 22, and 29 March). Basis for this categorization has been mentioned in details in subsequent sections.

3. Results

3.1. Time of *F* Layer Attaining the Peak Height and Spread *F* Onset Time

Zonal electric field is eastward during the day and westward during the night. Prior to its reversal during the evening hours, from eastward to westward, the zonal eastward electric field shows an enhancement. This enhancement of eastward electric field, prior to its reversal to westward, is termed as prereversal enhancement (PRE) of zonal electric field. Magnitude of this enhancement displays a day-to-day, seasonal, and solar cycle variations. This phenomenon has been studied in details, and several mechanisms have been proposed to explain its cause [e.g., *Farley et al*., 1986; *Haerendel and Eccles*, 1992]. Enhancement in the eastward electric field cause the postsunset height rise of the *F* layer. Height of the *F* layer in the postsunset hours rises till the time of zonal electric field turns westward, after which it descends. This height rise plays an important role in the generation of equatorial plasma bubble by enhancing the growth rate of the Rayleigh-Taylor (RT) instability. Also, the eastward electric field enhances the growth of the RT instability. Thus, the genesis of *F* region irregularity is expected to happen either at the time of *F* layer attaining the peak height or before it [*Abdu et al*., 1983; *Sastri et al*., 1997].

Figure 1 presents the distribution of peak *h'F* timing based on Sriharikota ionosonde observations corresponding to those nights when spread *F* has occurred. Out of the total 48 nights of continuous observations, spread *F* occurred on 30 nights (thus, the occurrence of spread *F* was ~62%). The time of *F* layer attaining the peak height varied between 19:00 IST and 20:30 IST. Here IST stands for the Indian Standard Time (UT + 5:30 h), which lags by ~8 min with respect to the local time at Sriharikota. Number of cases where the onset time of ESF coincided with the time of the *F* layer attaining the peak height is shown in green color in the histogram. In most of the nights, peak *h'F* was attained at or before 19:45 IST. In 10 out of 30 cases peak *h'F* was attained at 19:30 IST.

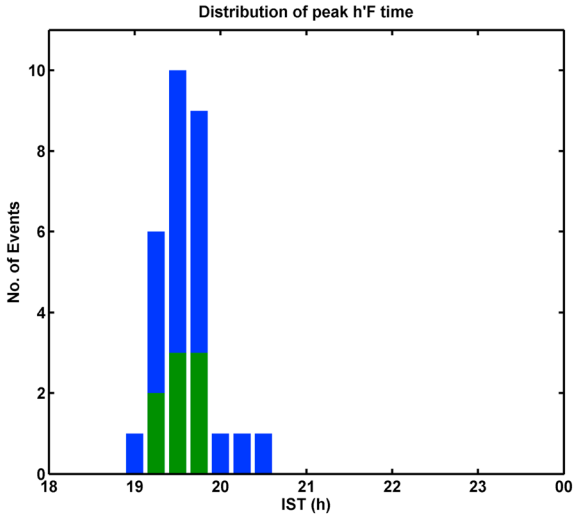

Figure 1. Histogram of the time of *F* layer attaining the peak height (peak *h'F* time), based on the ionosonde observations on spread *F* nights.

Growth of RT instability maximizes at a time when *F* region reaches peak height. Thus, the genesis of *F* region irregularities happens close to the time of *F* layer attaining the peak height. It becomes important to examine the time of spread *F* onset in the ionosonde observations. Figure 2 presents the distribution of the spread *F* onset time. It is interesting to see that distribution of spread *F* onset timing is quite different than that of the *F* layer attaining the peak height. While the peak height was attained by the *F* layer before 19:45 IST in most cases, spread *F* onset in the ionograms were observed after that.

3.2. Height Migration of *F* Layer in Early and Late Spread *F* Onset Cases

As presented earlier in Figures 1 and 2, it is evident that the onset of ESF always did not coincide with the time of *F* layer attaining the peak height. On a few cases onset of spread *F* was observed at the time of *F* layer attaining the peak height. On the other hand, there were cases where the onset of spread *F* was delayed by 15, 30, 45 min or even more than that, with respect to the peak *h'F* time. Height migration of *F* layer has been investigated in details corresponding to three different categories: early spread *F* onset cases, where the onset of spread *F* happened at or before the time of *F* layer attaining the peak height, moderately delayed spread *F* cases, where onset of spread *F* was observed after 30 min of *F* layer attaining the peak height, and late spread *F* onset cases, where the onset of spread *F* was delayed by 45 min or more with respect to the time of *F* layer attaining the peak height. Cases where the onset of spread *F* has been delayed by 15min have not been considered for the detailed analysis. This is because of the fact that the soundings were made every 15 min, and with this sampling rate it will not be possible to really characterize those cases into early or delayed spread *F* onset cases.

Figure 3a presents the *h'F* observed over Sriharikota corresponding to the early spread *F* onset cases. Here blue color line and symbol have been used to indicate the observation of classic *F* layer echo trace. Observation of spread *F* has been indicated by red color line and symbol. Average *h'F* value has been indicated by thick black line. One can see that the transition from blue to red color occurred at the time of *F* layer attaining the peak height (peak *h'F*). Here the peak *h'F* was attained at ~19:30 IST in most cases. Another interesting aspect is the enhanced level of *F* layer height rise. In most cases the peak *h'F* was more than 350 km, while the average peak *h'F* was ~350 km. Vertical plasma drift velocity has also been obtained using the ionosonde measurements. Vertical plasma drifts (V_Z) for the cases discussed above is presented in Figure 3b. Maximum V_Z in all the cases exceeded 20 m s^{-1}, and it became zero around 19:30 IST, indicating the reversal of electric field.

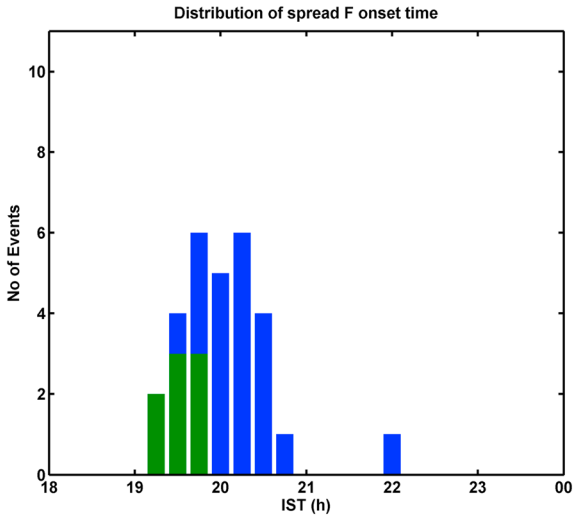

Figure 2. Histogram of the time of onset of ESF recorded in the ionograms.

F layer height variation and the V_Z corresponding to the moderately delayed spread *F* cases are indicated in Figures 3c and 3d, respectively. Peak *h'F* values in this category were in general less than those for the cases discussed in Figure 3a. Also, the peak vertical plasma drifts, V_Z, were in

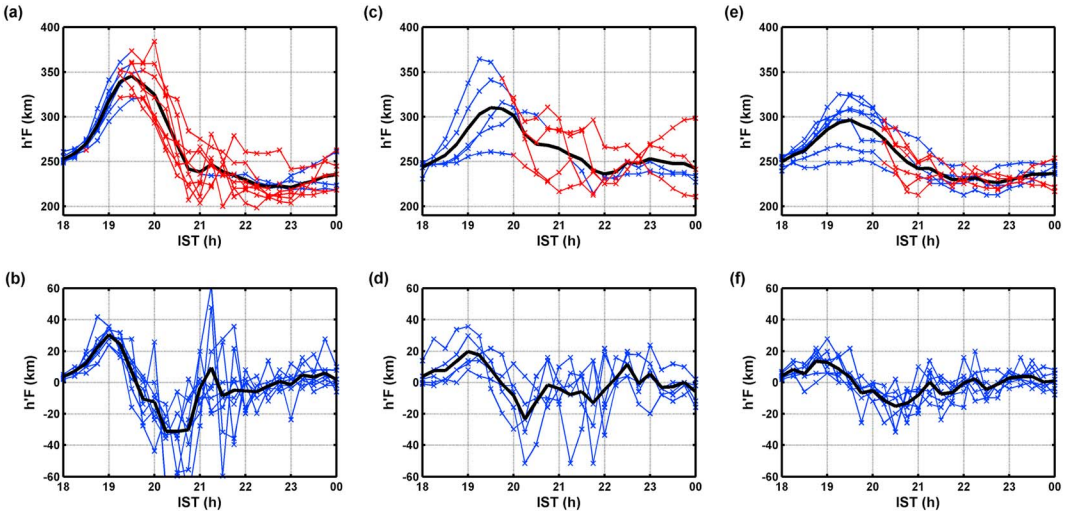

Figure 3. The (a) *h'F* and (b) V_Z, respectively, for early spread *F* onset cases. (c and d) The same as for Figures 3a and 3b but for the moderately delayed spread *F* onset cases. The (e) *h'F* and (f) V_Z, respectively, for the late onset cases. Blue color symbol/line has been used to indicate the presence of classical *F* layer trace, while red color symbol/line indicates spread *F*.

general less than those for the early spread *F* onset cases. Average peak *h'F* and peak V_Z in this case was also less than that corresponding to early spread *F* onset cases.

F layer height migration and the V_Z corresponding to the late spread *F* onset cases (where the onset of spread *F* was delayed by 45 min or more with respect to the time of *F* layer attaining the peak height) are presented in Figures 3e and 3f, respectively. Peak *h'F* for all the cases in this category was less than 350 km. Also, the average value of peak *h'F* was ~300 km. This value is ~50 km less than that for the early spread *F* onset cases. Also, the V_Z was quite less than that in the previous categories. However, on an average, the time of reversal of electric field (zero V_Z) was nearly similar in the three categories. Thus, in the second and third categories, the onset of spread *F* in the ionograms was observed during a time when zonal electric field was westward (V_Z negative). One can note that in a few nights corresponding to the second and third categories, the ESF has occurred despite insignificant height rise of the *F* layer. This is in accordance with the report by *Tsunoda et al.* [2010], of the ESF in the absence of *F* layer height rise but in the presence of LSWS. The peak height attained by the *F* layer and the peak V_Z associated with the prereversal enhancement of zonal field in the early (Category 1) and late (Category 3) spread *F* onset cases are also indicated in Table 1. For the early onset cases the peak V_Z and *h'F* were significantly larger than those for the late onset cases.

Table 1. Peak Vertical Plasma Drift (V_Z) and Peak *h'F* in Early and Late Spread *F* Onset Cases

Date	Peak V_Z (m/s)	Peak *h'F* (km)
	Early Spread F Onset Cases	
24 Feb 2004	25	322
6 Mar 2004	25	325
8 Mar 2004	36	350
19 Mar 2004	30	365
23 Mar 2004	35	360
24 Mar 2004	43	385
25 Mar 2004	35	355
27 Mar 2004	32	355
	Late Spread F Onset Cases	
21 Feb 2004	8	255
5 Mar 2004	13	269
13 Mar 2004	20	298
14 Mar 2004	21	310
20 Mar 2004	22	310
22 Mar 2004	24	328
29 Mar 2004	28	328

In Figure 3, while the mean V_Z in the three categories varied smoothly with time, individual cases show large fluctuations in V_Z. Particularly, the fluctuations in the V_Z occurred after the onset of ESF. It needs mention that after the onset of the ESF, height of the *F* layer in the ionosonde is basically represented by the minimum range of the *F* region irregularity. These irregularities are not spatially homogeneous and also drift eastward. As a result, it produces fluctuations in the *F* layer height measurement, which in turn creates fluctuations in the V_Z measurements.

Table 2. Ionogram Satellite Traces in Early and Late Spread *F* Onset Cases

Date	Satellite Trace Timing (IST)	2F Satellite Trace Timing (IST)
	Early Spread F Onset Cases	
24 Feb 2004	18:45, 19:30	18:45
6 Mar 2004	19:15	Nil
8 Mar 2004	19:00	Nil
19 Mar 2004	Nil	Nil
23 Mar 2004	19:15	Nil
24 Mar 2004	18:45	Nil
25 Mar 2004	19:00, 19:15	19:00
27 Mar 2004	19:30	Nil
	Late Spread F Onset Cases	
21 Feb 2004	Nil	Nil
5 Mar 2004	Nil	Nil
13 Mar 2004	Nil	Nil
14 Mar 2004	19:30, 19:45	Nil
20 Mar 2004	18:45, 19:30	Nil
22 Mar 2004	Nil	Nil
29 Mar 2004	Nil	Nil

3.2.1. Observation of Satellite Traces in the Ionograms

LSWS manifests in different forms in different observational techniques. Satellite traces in the ionograms and their relation to the formation of ESF have been evaluated by *Abdu et al.* [1981]. It has been found that the ESF is often preceded by the observation of satellite traces in the ionograms. Satellite traces appear different from the spread *F*. Often the satellite trace appears just above the 2F trace in the ionogram [*Tsunoda*, 2008], and it has also been regarded as a manifestation of the LSWS. Thus, ionosonde can enable one to observe the precursors of the ESF with ease and without much experimental complexities. Occurrence of satellite traces in the ionograms recorded at Sriharikota has also been analyzed. Table 2 presents the occurrence time of the satellite traces in the early (Category 1) and late (Category 3) spread *F* onset cases. Except on one night, satellite traces were observed prior to the ESF in the first category cases, while the satellite traces were observed only in two nights corresponding to the third category.

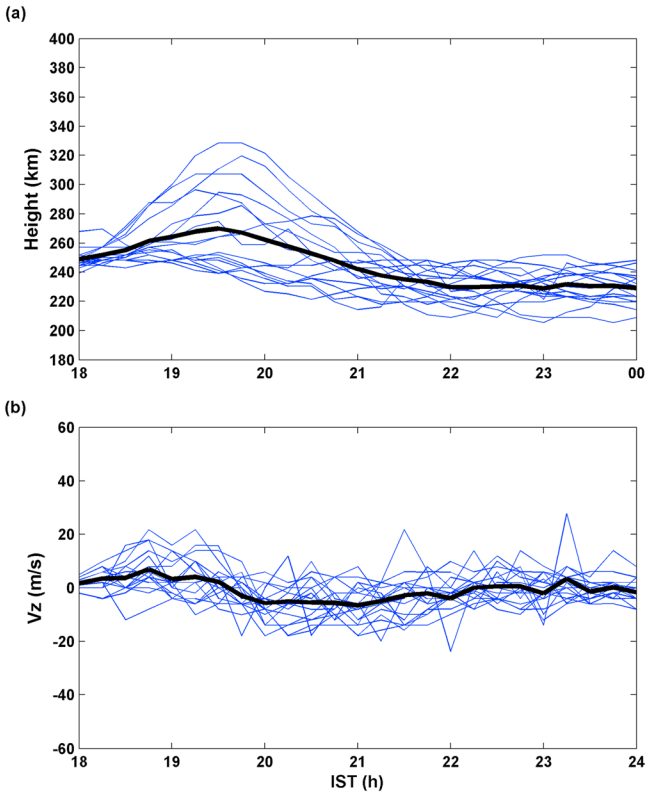

Figure 4. The (a) *h'F* and (b) V_Z on 18 non-spread *F* nights during 15 February to 2 April period.

3.3. *F* Layer Height Migration in Non-ESF Nights

Although, several investigations have highlighted the importance of LSWS in the formation of ESF, some investigations suggest the LSWS to be a necessary, may not be a sufficient condition for the formation of ESF [e.g., *Li et al.*, 2012]. It thus makes sense to also evaluate the height migration of *F* layer in non-ESF nights. Out of 48 nights of observations, ESF did not appear for 18 nights. *F* layer height migration (*h'F*) and the V_Z corresponding to the 18 non-ESF nights are shown in Figures 4a and 4b,

respectively. Although the *F* layer was found to attain the peak height as high as 340 km in some cases, in most nights, the *F* layer height rise was quite insignificant. Also, the V_Z values in the non-ESF nights were, in general, lesser than those for the ESF nights.

4. Discussion

This paper basically relates the onset time of the equatorial spread *F* and the post sunset height rise of the *F* layer. While the *F* layer was found to attain peak height (peak *h'F*) before 19:45 IST in most cases, the onset of spread *F* have not been observed to happen at that time in most cases. *Kelley et al*. [1979] discussed the generalized RT instability, where, in addition to the ion-neutral collision frequency and plasma density gradient, the zonal electric field also influences the growth rate of the RT instability. Eastward electric field acts similar to gravity in destabilizing the plasma; however, its contribution to the linear growth rate of the instability does not vary with the altitude. Thus, the genesis of the EPB is expected to happen either at a time when *F* layer reaches its peak altitude (peak *h'F*) or before that. Late onset of spread *F* most dominantly indicate the genesis of the EPB over a westward longitude, though fresh evolutionary type plasma bubble is also likely to be observed with a delay. Once originated, EPB drift eastward. Onset of spread *F* in the ionosonde depends whether the irregularities are present in the field of view of the ionosonde or not. Irregularities originating at a westward location will manifest as spread *F* at a time when they reach within the field of view of the ionosonde. Assuming the genesis of *F* region irregularities to have occurred at the peak *h'F* time, late onset of spread *F* indicates that the irregularities were not freshly generated. In fact, this is the most likely assumption, as the eastward electric field favors the onset of the RT instability; however, if the onset of the RT instability happens at a time when the zonal field is westward (i.e., after the *F* layer attaining the peak height), even a locally generated EPB will be observed with a delay with respect to the peak *h'F* time. Results presented in this manuscript are, however, discussed assuming that the onset of RT instability happens before peak *h'F* time.

Height migration, as well as vertical plasma drifts of the F layer, has been presented in Figure 3 for the early, moderately delayed, and late spread *F* onset cases. In the early onset cases the peak *h'F* over Sriharikota was, in general, more than that in the moderately delayed and late onset cases. Also, the average peak *h'F* corresponding to the first category was found to be ~35 km higher than that in the second category and ~50 km higher than in the third category. However, the time of *F* layer attaining the peak height was more or less similar in the three categories. The significant difference in the average peak *h'F* in the three categories can lead one to think of a zonal variation of peak *h'F*. This indicates the presence of a large-scale wave structure [*Tsunoda and white*, 1981]. It is quite plausible to think that in the early (moderately delayed and late) onset cases the crest (trough) of the standing large-scale wave structure was located above the ionosonde, i.e., over Sriharikota longitude. Irregularities, however, originated only close to the crest region and drifted eastward. Thus, in the second and third categories, the spread *F* irregularities were observed with a significant delay with respect to the time of *F* layer attaining the peak height. *Tsunoda and Ecklund* [2007] suggested that the extra eastward electric field component (in addition to the eastward electric field associated with the PRE of zonal field) associated with the LSWS can be the missing link in explaining the variability of ESF. Larger values of V_Z observed in the early spread *F* onset cases further corroborate the results of *Tsunoda and Ecklund* [2007]. In addition to it, the large-scale wave can produce a tilt in the ionosphere and can become unstable to wind-driven cross-field instability [*Kelley et al*., 1981; *Tsunoda*, 1983].

Previous investigations have indicated that the LSWS can originate much before the *F* region sunset time [*Thampi et al*., 2009; *Tsunoda et al*., 2011]. Thus, its detection was also made much before the onset of the ESF. Average vertical plasma drift (V_Z) in the early onset cases was slightly greater than that in the late onset cases, in the 18–19 IST periods itself (as shown in Figure 3). Thus, the observations presented in this manuscript are in compliance with those reported earlier. Also, *Tulasi Ram et al*. [2012, 2014a] have shown that the LSWS can be observed spatially a few degrees west of the *E* and *F* region sunset terminators (i.e., before the *E* and *F* region sunset times).

Several investigations have revealed that plasma bubble could also be of evolutionary type appearing around midnight [e.g., *Huang et al*., 2010; *Nishioka et al*., 2012]. However, such observations have been found to occur during the summer months (June, July, and August) of low to moderate solar activity periods. Also, the midnight spread *F* is often preceded by *F* layer height rise. In this manuscript, only the equinox period

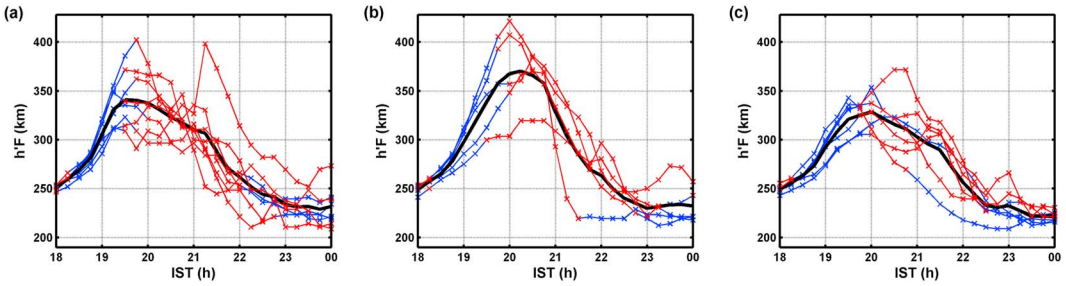

Figure 5. (a–c) The *h'F* recorded by Thumba ionosonde corresponding to the days discussed in Figure 3.

(February, March, and April) observations have been considered. During the equinox period, plasma bubbles are known to be generated at the time of the *F* layer attaining the peak height, when the ionosphere is most unstable under the RT instability. This is based on an assumption that the RT instability maximizes with the intensification of the zonal electric field associated with the prereversal enhancement. However, this assumption is likely to fail if the genesis of the EPB happens after the electric field reversal from eastward to westward. In such a scenario, locally generated fresh EPB will also be observed with a significant delay with respect to the peak *h'F* time. Results presented in this manuscript are indeed consistent with irregularities generated to the west and then drifting into the field of view of the Sriharikota ionosonde, but this cannot be proven for all cases considering the experimental limitations. This assumption can be verified using simultaneous Airglow imager and ionosonde observations as the longitudinal origin of the EPB can be exactly determined using the airglow imager, while ionosonde can be utilized to measure the *F* layer height.

Another important aspect related with the early manifestation of the LSWS is the appearance of the satellite traces in the ionograms. Timings of the appearance of satellite traces in the ionograms, in the two cases, have been indicated in Table 2. One can note that, while satellite trace was not seen only on one night in the first category, it was observed only on two nights corresponding to the third category. Lesser appearance of satellite traces in the third category also gives some indication that the corrugations in the *F* layer responsible for satellite traces were not located overhead (within the field of view of the ionosonde). It gives an impression that in the third category cases it was the trough of the large-scale wave that was located over Sriharikota, while in the first category the soundings were made of a region located in the vicinity of the crest of the large-scale wave.

Observations corresponding to 18 non-ESF nights have also been presented in Figure 4. The *F* layer height rise in non-ESF cases (Figure 4a) has some resemblance with the late spread *F* onset cases (Figure 3e). Five of the non-ESF cases have the peak *h'F* comparable to or larger than the average peak *h'F* of late spread *F* onset cases. This implies that, while the *F* layer height plays the most dominant role in the EPB genesis, it alone does not determine the occurrence of the EPB. Might be, in the five non-ESF cases with significant *F* layer height rise, bottomside sinusoidal zonal plasma density variation capable of seeding the RT instability was absent. Thus, the seeding is likely to be as important a factor as the *F* layer height. Recently, *Li et al.* [2012] have indicated that the seed perturbation alone is not the sufficient criterion for the ESF to occur, as the *F* layer height rise plays a dominant role. Thus, the results presented in this manuscript are in good accordance with *Li et al.* [2012]. Occurrence of the EPB is likely to depend on more than one parameter, including the *F* layer height, seed perturbation, and the LSWS.

4.1. *F* Layer Height Migration Over Thumba

Spatial observation of *F* layer height rise can play an important role in resolving the spatial LSWS features. However, it will be limited by the spatial separation between the observing stations and the scale size of the LSWS. Thumba (8.53°N, 76.87°E) is an equatorial (magnetic equator) station in India and is located ~360 km west of Sriharikota and houses a digital ionosonde. Although there exists a latitudinal difference of ~7° between Sriharikota and Thumba, simultaneous ionosonde observations from these locations can still be used to observe the longitudinal differences in the postsunset height rise of *F* layer. Thus, to study the longitudinal feature of the *F* layer height rise, the height migration of the *F* layer over Thumba (based on Thumba ionosonde observations) has been examined for the cases discussed in Figure 3. Figure 5 shows the

h′F observed over Thumba corresponding to the nights discussed in Figure 3. Figure 5a shows the *h*′*F* over Thumba corresponding to the early onset cases discussed in Figure 3a; *h*′*F* over Thumba corresponding to the moderately delayed spread *F* cases discussed in Figure 3b has been indicated in Figure 5b. The *h*′*F* over Thumba corresponding to the late spread *F* cases discussed in Figure 3c is shown in Figure 5c. Two of the important aspects of the Thumba observations are as follows: (1) spread *F* onset in all the three categories occurred mostly at the time of *F* layer attaining the peak height and (2) the relative magnitude of *F* layer height rise in the three categories differed from that in Figure 3. As far as the onset time of ESF is concerned, ionosonde located at magnetic equator is more likely to observe the bottom type spread F prior to the occurrence of topside spread *F* (which may not be the case with the low-latitude observation). Coming to the *F* layer height rise over Thumba; unlike in Figure 3, where category 1 cases attained the maximum height, in Figure 5, the maximum height was attained by the category 2 cases. The cases belonging to the third category displayed the least average height rise over Thumba, as shown in Figure 5c. Thus, it gives us some indication that in the first category cases, the crest (trough) of the large-scale wave was located in the vicinity of Sriharikota (Thumba) longitude, whereas in the second category cases, the trough (crest) of the large-scale wave was located in the vicinity of Sriharikota (Thumba) longitude, as supported by the fact that average height rise of Category 1 (Category 2) cases was maximum in Figure 3 (Figure 5).

Another important aspect is that the average peak *h*′*F* over Sriharikota, corresponding to the third category (where the onset of the ESF over Sriharikota was delayed by more than 45 min with respect to the peak *h*′*F* time), was ~50 km less than that corresponding to the first category (as can be seen in Figure 3), whereas over Thumba, the average peak *h*′*F* difference between the first and the third categories was just ~10 km (as can be seen in Figure 5). Possibly, in the third category cases, the zonal separation of the crest and the trough of the concerned large-scale wave was significantly larger than the zonal separation between Thumba and Sriharikota (i.e., 360 km). This possibility is further corroborated by the fact that spread *F* onset over Sriharikota in the third category happened after a larger delay with respect to the peak *h*′*F* time than that in the second category. This is just one possibility, which cannot be verified by just two zonally separated ionosondes. Continuous observations using three or more zonally separated ionosondes will be required to derive the exact structure of the LSWS; however, such a network of ionosonde does not exist. Nonetheless, the difference in the Sriharikota and Thumba *h*′*F* observations, corresponding to the three different categories, still indicates that the height rise of the *F* layer was not zonally uniform. This in turn gives some indications of the presence of large-scale wave.

5. Summary and Concluding Remarks

The time of *F* layer attaining the peak height (peak *h*′*F*), the onset time of spread *F* and its relation with the peak *h*′*F* have been investigated using the Sriharikota ionosonde observations of 15 February 2004 to 2 April 2004 (48 days) period. The distribution of peak *h*′*F* time and spread *F* onset time differed significantly, indicating that the time of spread *F* onset in many cases differed from the time of *F* layer attaining the peak height. Average peak *h*′*F* in the early spread *F* onset cases was found to be ~50 km, more than that in the late spread *F* onset cases. This can be explained if a standing large-scale wave structure is assumed to exist in the bottomside of *F* layer. However, the exact magnitude of the large-scale wave on a particular evening can only be inferred using the zonal measurement of *F* layer height. Other popular techniques like satellite traces, multireflected echo traces, scanning airglow photometers, and total electron content measurements using C/NOFS (Communication and Navigation Outages forecasting system) can also be used to monitor the presence of large-scale waves. However, these techniques provide an integrated picture and scarcely reveal the precise structure of the large-scale waves in terms of its amplitude and *F* layer height. Thus, the continuous zonal measurement of *F* layer height will be required to infer the exact structure of the large-scale wave (amplitude, phase, and height) and its impact on the stability of the evening *F* layer.

Acknowledgments

The author is thankful to Indian Institute of Geomagnetism for providing Nanabhoy Moos postdoctoral fellowship. The author is also grateful to A.K. Patra for providing the Sriharikota ionosonde data. Sriharikota and Thumba ionosonde data can be obtained by contacting A.K. Patra (akpatra@narl.gov.in) and T.K. Pant (tarun_kumar@vssc.gov.in), respectively.

References

Abdu, M. A., I. S. Batista, and J. A. Bittencourt (1981), Some characteristics of spread *F* at the magnetic equatorial station Fortaleza, *J. Geophys. Res.*, *86*(A8), 6836–6842, doi:10.1029/JA086iA08p06836.

Abdu, M. A., R. T. deMedeiros, J. A. Bittencourt, and I. S. Batista (1983), Vertical ionization drift velocities and range type spread *F* in the evening equatorial ionosphere, *J. Geophys. Res.*, *88*(A1), 399–402, doi:10.1029/JA088iA01p00399.

Aquino, M., and V. Sreeja (2013), Correlation of scintillation occurrence with interplanetary magnetic field reversals and impact on Global Navigation Satellite System receiver tracking performance, *Space Weather*, *11*, 219–224, doi:10.1002/swe.20047.

Bagiya, M. S., R. Sridharan, and S. Sunda (2013), Pre-assessment of the "strength" and "latitudinal extent" of L-band scintillation: A case study, *J. Geophys. Res. Space Physics*, *118*, 488–495, doi:10.1029/2012JA017989.

de Lima, G. R. T., S. Stephany, E. R. de Paula, I. S. Batista, M. A. Abdu, L. F. C. Rezende, M. G. S. Aquino, and A. P. S. Dutra (2014), Correlation analysis between the occurrence of ionospheric scintillation at the magnetic equator and at the southern peak of the equatorial ionization anomaly, *Space Weather*, *12*, 406–416, doi:10.1002/2014SW001041.

Farley, D. T., E. Bonelli, B. G. Fejer, and M. F. Larsen (1986), The prereversal enhancement of the zonal electric field in the equatorial ionosphere, *J. Geophys. Res.*, *91*(A12), 13,723–13,728, doi:10.1029/JA091iA12p13723.

Haerendel, G., and J. V. Eccles (1992), The role of the equatorial electrojet in the evening ionosphere, *J. Geophys. Res.*, *97*(A2), 1181–1192, doi:10.1029/91JA02227.

Huang, C.-S., O. de La Beaujardiere, R. F. Pfaff, J. M. Retterer, P. A. Roddy, D. E. Hunton, Y.-J. Su, S.-Y. Su, and F. J. Rich (2010), Zonal drift of plasma particles inside equatorial plasma bubbles and its relation to the zonal drift of the bubble structure, *J. Geophys. Res.*, *115*, A07316, doi:10.1029/2010JA015324.

Huang, C.-S., O. de La Beaujardière, P. A. Roddy, D. E. Hunton, J. O. Ballenthin, M. R. Hairston, and R. F. Pfaff (2013), Large-scale quasiperiodic plasma bubbles: C/NOFS observations and causal mechanism, *J. Geophys. Res. Space Physics*, *118*, 3602–3612, doi:10.1002/jgra.50338.

Kelley, M. C., K. D. Baker, and J. C. Ulwick (1979), Late time barium cloud striations and their possible relationship to equatorial spread *F*, *J. Geophys. Res.*, *84*(A5), 1898–1904, doi:10.1029/JA084iA05p01898.

Kelley, M. C., M. F. Larsen, C. LaHoz, and J. P. McClure (1981), Gravity wave initiation of equatorial spread *F*: A case study, *J. Geophys. Res.*, *86*(A11), 9087–9100, doi:10.1029/JA086iA11p09087.

Kelly, M. A., J. M. Comberiate, E. S. Miller, and L. J. Paxton (2014), Progress toward forecasting of space weather effects on UHF SATCOM after Operation Anaconda, *Space Weather*, *12*, 601–611, doi:10.1002/2014SW001081.

Li, G., B. Ning, M. A. Abdu, W. Wan, and L. Hu (2012), Precursor signatures and evolution of post-sunset equatorial spread-*F* observed over Sanya, *J. Geophys. Res.*, *117*, A08321, doi:10.1029/2012JA017820.

Nishioka, M., Y. Otsuka, K. Shiokawa, T. Tsugawa, Effendy, P. Supnithi, T. Nagatsuma, and K. T. Murata (2012), On post-midnight field-aligned irregularities observed with a 30.8-MHz radar at a low latitude: Comparison with *F*-layer altitude near the geomagnetic equator, *J. Geophys. Res.*, *117*, A08337, doi:10.1029/2012JA017692.

Oladipo, O. A., J. O. Adeniyi, A. O. Olawepo, and P. H. Doherty (2014), Large-scale ionospheric irregularities occurrence at Ilorin, Nigeria, *Space Weather*, *12*, 300–305, doi:10.1002/2013SW000991.

Patra, A. K., A. Taori, P. P. Chaitanya, and S. Sripathi (2013), Direct detection of wavelike spatial structure at the bottom of the *F* region and its role on the formation of equatorial plasma bubble, *J. Geophys. Res. Space Physics*, *118*, 1196–1202, doi:10.1002/jgra.50148.

Sastri, J. H., M. A. Abdu, I. S. Batista, and J. H. A. Sobral (1997), Onset conditions of equatorial (range) spread *F* at Fortaleza, Brazil, during the June solstice, *J. Geophys. Res.*, *102*(A11), 24,013–24,021, doi:10.1029/97JA02166.

Shume, E. B., A. J. Mannucci, M. D. Butala, X. Pi, and C. E. Valladares (2013), Flux tube analysis of L-band ionospheric scintillation, *J. Geophys. Res. Space Physics*, *118*, 3791–3804, doi:10.1002/jgra.50285.

Sreeja, V., M. Aquino, and Z. G. Elmas (2011), Impact of ionospheric scintillation on GNSS receiver tracking performance over Latin America: Introducing the concept of tracking jitter variance maps, *Space Weather*, *9*, S10002, doi:10.1029/2011SW000707.

Sreeja, V., M. Aquino, Z. G. Elmas, and B. Forte (2012), Correlation analysis between ionospheric scintillation levels and receiver tracking performance, *Space Weather*, *10*, S06005, doi:10.1029/2012SW000769.

Thampi, S. V., M. Yamamoto, R. T. Tsunoda, Y. Otsuka, T. Tsugawa, J. Uemoto, and M. Ishii (2009), First observations of large-scale wave structure and equatorial spread *F* using CERTO radio beacon on the C/NOFS satellite, *Geophys. Res. Lett.*, *36*, L18111, doi:10.1029/2009GL039887.

Tsunoda, R. T. (1983), On the generation and growth of equatorial backscatter plumes: 2. Structuring of the west walls of upwellings, *J. Geophys. Res.*, *88*(A6), 4869–4874, doi:10.1029/JA088iA06p04869.

Tsunoda, R. T. (2008), Satellite traces: An ionogram signature for large-scale wave structure and a precursor for equatorial spread *F*, *Geophys. Res. Lett.*, *35*, L20110, doi:10.1029/2008GL035706.

Tsunoda, R. T. (2009), Multi-reflected echoes: Another ionogram signature of large-scale wave structure, *Geophys. Res. Lett.*, *36*, L01102, doi:10.1029/2008GL036221.

Tsunoda, R. T., and W. L. Ecklund (2007), On the post-sunset rise of the equatorial *F* layer and superposed upwellings and bubbles, *Geophys. Res. Lett.*, *34*, L04101, doi:10.1029/2006GL028832.

Tsunoda, R. T., and B. R. White (1981), On the generation and growth of equatorial backscatter plumes: 1. Wave structure in the bottomside *F* layer, *J. Geophys. Res.*, *86*(A5), 3610–3616, doi:10.1029/JA086iA05p03610.

Tsunoda, R. T., D. M. Bubenik, S. V. Thampi, and M. Yamamoto (2010), On large-scale wave structure and equatorial spread *F* without a post-sunset rise of the *F* layer, *Geophys. Res. Lett.*, *37*, L07105, doi:10.1029/2009GL042357.

Tsunoda, R. T., M. Yamamoto, T. Tsugawa, T. L. Hoang, S. Tulasi Ram, S. V. Thampi, H. D. Chau, and T. Nagatsuma (2011), On seeding, large-scale wave structure, equatorial spread *F*, and scintillations over Vietnam, *Geophys. Res. Lett.*, *38*, L20102, doi:10.1029/2011GL049173.

Tulasi Ram, S., P. V. S. Rama Rao, D. S. V. V. D. Prasad, K. Niranjan, S. Gopi Krishna, R. Sridharan, and S. Ravindran (2008), Local time dependant response of post-sunset ESF during geomagnetic storms, *J. Geophys. Res.*, *113*, A07310, doi:10.1029/2007JA012922.

Tulasi Ram, S., M. Yamamoto, R. T. Tsunoda, S. V. Thampi, and S. Gurubaran (2012), On the application of differential phase measurements to study the zonal large scale wave structure (LSWS) in the ionospheric electron content, *Radio Sci.*, *47*, RS2001, doi:10.1029/2011RS004870.

Tulasi Ram, S., M. Yamamoto, R. T. Tsunoda, H. D. Chau, T. L. Hoang, B. Damtie, M. Wassaie, C. Y. Yatini, T. Manik, and T. Tsugawa (2014a), Characteristics of large-scale wave structure observed from African and Southeast Asian longitudinal sectors, *J. Geophys. Res. Space Physics*, *119*, 2288–2297, doi:10.1002/2013JA019712.

Tulasi Ram, S., S. Kumar, S.-Y. Su, B. Veenadhari, and S. Ravindran (2014b), The influence of Corotating Interaction Region (CIR) driven geomagnetic storms on the development of equatorial plasma bubbles (EPBs) over wide range of longitudes, *Adv. Space Res.*, *55*, 535–544, doi:10.1016/j.asr.2014.10.013.

Whalen, J. A. (2007), Weather of the postsunset equatorial anomaly recorded daily during 2 years near solar maximum, *Space Weather*, *5*, S01002, doi:10.1029/2006SW000235.

Zhang, D. H., Z. Xiao, M. Feng, Y. Q. Hao, L. Q. Shi, G. L. Yang, and Y. C. Suo (2010), Temporal dependence of GPS cycle slip related to ionospheric irregularities over China low-latitude region, *Space Weather*, *8*, S04D08, doi:10.1029/2008SW000438.